THE JOURNAL OF PHYSICAL CHEMISTRY C
A JOURNAL OF THE AMERICAN CHEMICAL SOCIETY

pubs.acs.org/JPCC

Article

Characterization of Substrates and Surface-Enhancement in Atomic Force Microscopy Infrared Analysis of Amyloid Aggregates

Stanislav Rizevsky, Kiryl Zhaliazka, Tianyi Dou, Mikhail Matveyenka, and Dmitry Kurouski*

Cite This: https://doi.org/10.1021/acs.jpcc.1c09643

Read Online

ACCESS | Metrics & More | Article Recommendations | Supporting Information

ABSTRACT: Atomic force microscopy infrared (AFM-IR) spectroscopy is an emerging analytical technique that can be used to probe the structural organization of specimens with nanometer spatial resolution. A growing body of evidence suggests that nanoscale structural analysis of very small (<10 nm) biological objects, such as viruses and amyloid aggregates, requires substrates that must fit strict criteria of low surface roughness and low IR background, simultaneously. In this study, we examine the suitability of a broad range of substrates commonly used in AFM and IR fields, and we determined that silicon, zinc sulfide, and calcium fluoride are the most ideal substrates for nanoscale imaging of amyloid oligomers, protein aggregates that are directly linked to the onset and progression of neurodegenerative diseases. Our data show that these substrates provide the lowest roughness and the lowest background in the 800−1800 cm^{-1} spectral window from all examined AFM and IR substrates. We also investigate a contribution of surface enhancement in AFM-IR by the direct comparison of signal intensities from oligomers located on silicon and gold-coated silicon surfaces. We found that metallization of such substrates provides a factor of ∼7 enhancements to the IR signal and induces an equivalent enhancement of the sample background in the 950−1250 cm^{-1} spectral region.

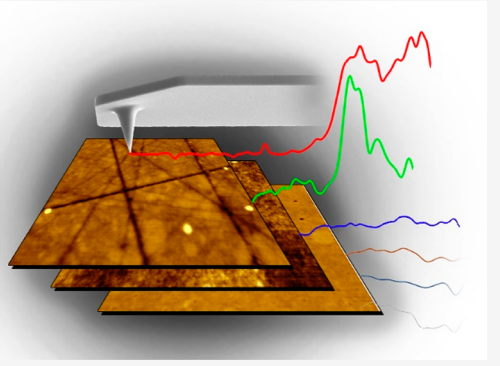

INTRODUCTION

Infrared (IR) spectroscopy is commonly used to analyze the chemical structure of a broad range of samples ranging from food supplies to forensic specimens.[1−5] This is primarily due to the (i) noninvasive and nondestructive nature of IR, (ii) low instrumental costs, (iii) high sensitivity, and (iv) rapid development of computational approaches that enable the prediction of IR spectra based on the chemical structure of the analyte.[6−10] Over the past decade, substantial instrumental development enabled the miniaturization of IR spectrometers,[11,12] as well as a development of IR microscopes that can provide ∼10 mm spatial resolution in the chemical imaging of analyzed samples.[13,14]

Coupling of IR with atomic force microscopy (AFM) can push the spatial resolution far beyond the light diffraction limit.[15] In this spectroscopic approach, known as atomic force microscopy infrared (AFM-IR) spectroscopy, a frequency of the pulsed tunable IR laser is tuned into the resonance with the vibrational frequency of sample molecules.[16−18] Absorbed IR radiation causes thermal expansions that are recorded by a metallized scanning probe positioned on the sample surface. If the laser repetition rate matches the contact frequency of the AFM scanning probe, nearly 2 orders of magnitude signal enhancement can be achieved.[19] This enhancement can be further improved by the metallization of scanning probes and sample surfaces.[20,21] Probe metallization is used to minimize the IR absorption by silicon or silicon nitride, as well as to direct and localize the electric field at the probe apex, a phenomenon that is known as the "lightning rod" effect.[22,23] It should be noted that, if a total internal reflection (TIR) is used for the probe illumination, the generated evanescent field minimizes the probe absorption.[24] Scattered pieces of experimental evidence suggest that substrate metallization can also provide substantial enhancement to the IR spectra.[25,26] However, the exact contribution of substrate-based enhancement in AFM-IR remains unclear.

Over the past decade, AFM-IR was extensively used for the structural characterization of relatively thick (>500 nm) samples of minerals and synthetic materials, such as boron−nitride films, polyethylenes, and perovskites.[27−31] This sample thickness minimizes the importance of both the chemical nature of the underlying substrates and the effect of their metallization.

Rapid development of AFM-IR for biological research requires a better understanding of the impact of the (i) chemical nature, (ii) roughness, and (iii) metallization of substrates used for the imaging of thin (<10 nm) protein samples such as amyloid oligomers and fibrils.[32−36] These

Received: November 8, 2021
Revised: February 7, 2022

protein aggregates are directly linked to a large variety of amyloidogenic diseases, including Alzheimer's and Parkinson's diseases, as well as diabetes type 2.[37,38] The structural characterization of these protein aggregates provides a wealth of information about the molecular mechanisms that determine their formation. For instance, Ruggeri utilized AFM-IR to unravel the influence of pathogenic mutations on the aggregation of α-synuclein (α-Syn).[39,40] It was found that mutations of α-Syn result in the formation of structurally different amyloid fibril polymorphs compared to fibrils formed from a wild-type protein.[40] Zhou and Kurouski used AFM-IR to examine the structural organization of α-Syn oligomers, protein aggregates that later propagate into insoluble fibrils.[41] AFM-IR revealed at least two different classes of α-Syn oligomers that dominated by α-helical/unordered structure and antiparallel- and parallel-β-sheets. The first type of oligomers remained unchanged during the course of protein aggregation, whereas the antiparallel β-sheet was rearranged into a parallel-β-sheet secondary in the second type of oligomers upon their propagation into fibrils.[41] This structural analysis of protein aggregates can be done based on the amide I and II regions of their spectrum, which stretches from 1500 to 1700 cm^{-1}.[26,33,35,39] Recently reported experimental results by our groups show that the 800−1300 cm^{-1} spectral region can be critically important for the elucidation of protein−lipid interactions.[42] Such interactions can uniquely alter the aggregation rates of proteins, as well as the secondary structure of amyloid oligomers and fibrils.[43]

Expanding upon these findings, we propose to investigate the suitability of a broad range of AFM and IR substrates for the artifact-free structural characterization of protein oligomers within the 800 to 1700 cm^{-1} spectral range. This analysis is performed through the prism of accessibility and costs of currently available IR and AFM substrates.

MATERIALS AND METHODS

Materials. Mica and calcium fluoride (CaF_2) were purchased from Ted Pella (Redding, CA, U.S.A.); sapphire, potassium bromide (KBr), and zinc oxide (ZnO) were purchased from MSE Supplies LLC (Tucson, AZ, U.S.A.); zinc sulfide (ZnS) and silicon nitride (Si_3N_4) were purchased from Bruker Nano (Santa Barbara, CA, U.S.A.); silicon (Si) was purchased from Fluoroware Inc. (Billerica, MA, U.S.A.); and glass coverslips were purchased from Thermo Fihser Scientific (Waltham, MA). The information about the substrates provided by the vendor is summarized in Table S1. Insulin was purchased from Sigma-Aldrich (St. Louis, MO, U.S.A.), and 1,2-dimyristoyl-*sn*-glycero-3-phosphocholine (DMPC) was purchased from Avanti (Birmingham, AL, U.S.A.).

To determine the average substrate roughness (Ra), root-mean-square roughness (Rq), maximum peak to valley roughness (Ry), and Scratch/Dig values, five different substrate samples were analyzed using AFM; a 1 × 1 μm substrate area was analyzed for each substrate. Data analysis was made in Gwyddion 2.59. The obtained values are summarized in the Table S2.

Protein Aggregation. Insulin was aggregated in a lipid-free environment and in the presence of DMPC at a 1:1 lipid to protein ratio at 37 °C under constant agitation in a Tecan Spark plate reader (Männedorf, Switzerland) at 510 rpm. After 24 h of agitation, samples were cooled to room temperature. Next, the sample aliquot was diluted with distilled water, place on the substrate, and dried under room temperature.

AFM Imaging. AFM imaging was performed on a AIST-NT-HORIBA system (Edison, NJ) using silicon AFM probes with a related parameters force constant of 2.7 N/m and a resonance frequency of 50−80 kHz that were purchased from Appnano (Mountain View, CA). The analysis of the collected images was performed using AIST-NT software (Edison, NJ).

AFM-IR. AFM-IR imaging was conducted using a Nano-IR3 system (Bruker Nano, Santa Barbara, CA, U.S.A.). The IR source was a QCL laser. Contact-mode AFM tips (ContGB-G AFM probe, NanoAndMore) were used to obtain all spectra. On average, 15 spectra were collected from each substrate and protein sample; 2 cm^{-1} spectral resolution was used. Treatment and analysis of the collected spectra were performed in Analysis Studio software. The spectra were treated with a Savitzky−Golay filter (2 polynomial order and 7 side points).

Metal Deposition. Gold (99.99% Kurt J. Lesker, Efferson Hills, PA, U.S.A.) was thermally evaporated in a MBrown system (MBrown, Stratham, NH) onto substrates at a constant of 0.2 $A{\cdot}s^{-1}$ rates under ~1 × 10^{-6} mbar. After 80 nm of Au was deposited on the substrates, the evaporation was stopped and the cooling down was continued until room temperature was reached.

Thermal Annealing. Silicon wafers with 85 nm of Au film on their surfaces were placed into a furnace that was kept at 450 °C for 30 and 60 min. Next, substrates were cooled down to room temperature and analyzed using AFM.

RESULTS AND DISCUSSION

AFM and AFM-IR Analyses of the Substrates. One can expect that an ideal substrate for AFM-IR imaging of amyloid aggregates must match strict criteria of AFM and IR, possess minimal surface roughness to enable morphological identification of small, 3−5 nm, protein aggregates, and have low, if any, IR background. We used AFM to examine the topography and surface roughness of the following most commonly used AFM and IR substrates: mica, glass, Si_3N_4, Si, ZnO, CaF_2, sapphire, and ZnS; see Figure 1.

We found that mica, glass, Si_3N_4, Si, ZnO, and CaF_2 had smooth surfaces that were perfectly suitable for AFM imaging of oligomers. We have also found that surfaces of CaF_2 and ZnO had long clearly defined grooves that decrease the quality of the substrates, but did not result in a substantial increase in the surface roughness. Our findings also show that mica exhibit the lowest surface roughness, whereas glass, Si_3N_4, Si, and ZnO have 2× higher surface roughness than mica. We have also found that sapphire and ZnS exhibit a highly rough surface with lots of spherical aggregates present that highly likely originate from the polishing methods used to fabricate these substrates. This surface analysis suggests that it is unlikely that sapphire and ZnS can be used for AFM-IR imaging of amyloid aggregates. At the same time, mica, glass, Si_3N_4, Si, ZnO, and CaF_2 are perfectly suitable for AFM-IR imaging of small protein aggregates.

Next, we examined the IR background signals of these substrates using AFM-IR. We have found that CaF_2, SnZ, Si, ZnO, and sapphire, as well as KBr, have very little if any IR background signal within 800−1800 cm^{-1}, see Figure 2. It should be noted that, although analyzed, KBr presents very little, if any, suitability to the biological research due to the high solubility of the substrate in water. This substantially

https://doi.org/10.1021/acs.jpcc.1c09643
J. Phys. Chem. C XXXX, XXX, XXX−XXX

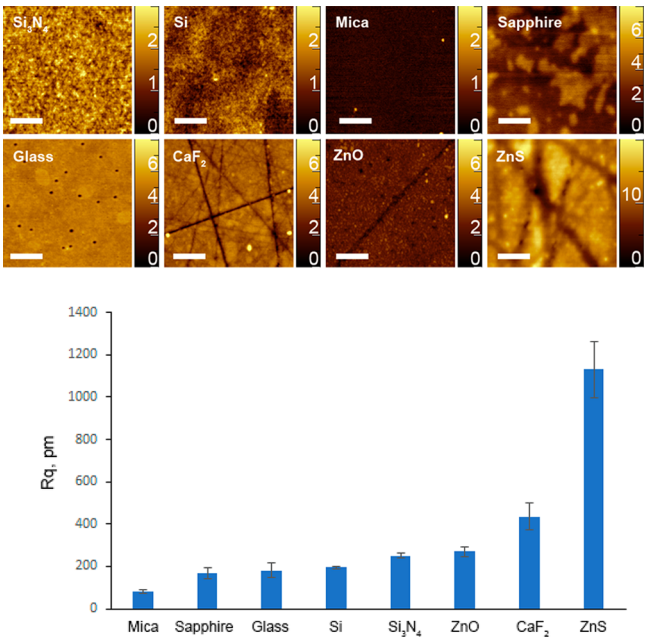

Figure 1. AFM images (top) of Si_3N_4, Si, mica, sapphire, glass, CaF_2, ZnO, and ZnS and a diagram (bottom) of the root-mean-square roughness (Rq) of their surfaces. Scale bar is 250 nm.

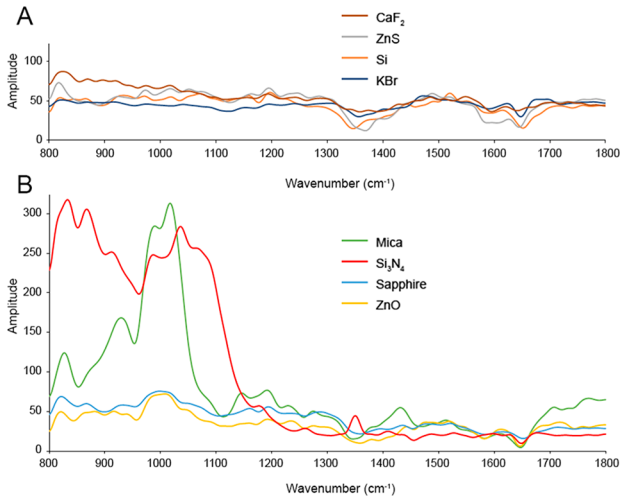

Figure 2. AFM-IR spectra of bare CaF_2, ZnO, Si, and KBr (A), as well as mica, Si_3N_4, sapphire, and ZnS.

complicates the use of this substrate for the deposition of water-soluble protein aggregates. At the same time, we found that Si_3N_4 and mica exhibit a very strong background in the 1100−800 cm^{-1} region. These findings show that both Si_3N_4 and mica can be used for the AFM-IR analysis of amyloid aggregates grown in the lipid-free environment. However, these substrates unlikely can be used if the information about the lipid composition is expected to be revealed, because lipids exhibit vibrational modes in this (800−1100 cm^{-1}) spectral region.[42]

Considering the commercial costs of the substrates analyzed in our study, we found that Si, CaF_2, and ZnS are the best candidates for AFM-IR imaging of amyloid aggregates, see Table 1. Finally, although glass coverslips have a very low surface roughness and IR background, their use in AFM-IR is limited by the strong absorption properties of IR light by the

Table 1. Results of AFM and AFM-IR Analyses of the Surface Roughness and IR Background of the Examined Substrates

substrate	surface roughness	IR background	cost	other properties
glass	low	low	low	absorbs IR
Si	low	low	low	not observed
Si_3N_4	low	high	low	not observed
mica	very low	high	low	can be cleaved and reused
ZnS	high	low	medium	not observed
ZnO	low	low	high	not observed
sapphire	high	low	high	not observed
CaF_2	low	low	medium	not observed
KBr	low	low	low	water-soluble

glass. This drastically minimizes the thermal expansion of the protein specimens deposited on it.

Elucidation of the Effect of Substrate Metallization. We evaporated 85 nm of Au on the surface of Si, CaF_2 and ZnO and examined their surfaces using AFM. We found that metal deposition results in the formation of a grain-like surface that is poorly suitable for AFM-IR imaging of amyloid aggregates. We used thermal annealing to determine the extent to which such grain-like surfaces can be flattened. Previously, our group demonstrated that, at ∼400 °C, Au atoms can move across the metallic surfaces, which drastically changes the shapes of the Au nanostructures.[44] Our experimental findings show that, after Si is coated with 85 nm of Au and exposed for 30 min at 450 °C, the RMS of the surface roughness decreased from 1.39 to 0.73 nm. Prolonged heating only slightly decreased the surface roughness (0.5 nm after 60 min at 450 °C), whereas we observed the formation of large cracks on the metallic surface, Figure 3. These findings demonstrate that 30−60 min long annealing of substrates at mild temperatures can be used to decrease the roughness of the metallic films on their surfaces.

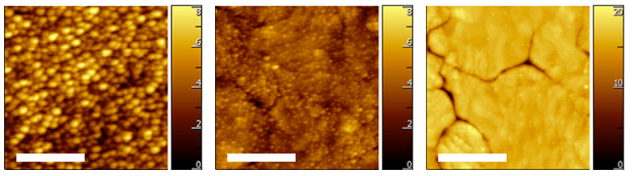

Figure 3. AFM images of the Si substrate coated with 85 nm of Au before thermal annealing (A) and after 30 min (B) and 60 min (C) of exposure at 450 °C.

Spectroscopic analysis of Au-coated and bare Si, ZnS, and CaF_2 substrates revealed that metal coating causes a drastic increase in the intensity of the spectral background within the 950−1250 cm^{-1} region, Figure 4. We have also observed an increase in the intensity of the 1650−1750 cm^{-1} region. It should be noted that all three chemically different substrates exhibited highly similar spectral profiles in these spectral regions. These findings suggest that the corresponding spectral changes could be caused by the silicon of the scanning probes.

Although the exact physical origin of this Au-induced background enhancement is unclear, these results suggest that it is unlikely that the Au coating can be used for AFM-IR imaging of lipid-containing amyloid aggregates due to the presence of lipid vibrations within the 950−1250 cm^{-1} spectral

https://doi.org/10.1021/acs.jpcc.1c09643
J. Phys. Chem. C XXXX, XXX, XXX−XXX

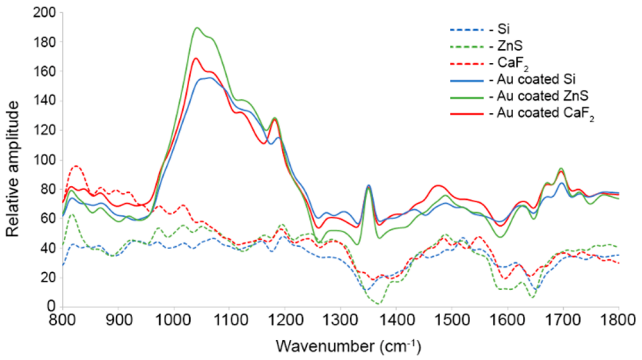

Figure 4. AFM-IR spectra of bare (dashed lines) and Au-coated Si, ZnS, and CaF_2 substrates.

region. These data also suggest that metallization of substrates may cause artifacts in the amide I and II regions of the spectra collected from protein aggregates deposited on them. To verify this, we collected spectra from the same amyloid aggregates deposited onto bare Si and Au-coated Si, see Figures 5 and S3.

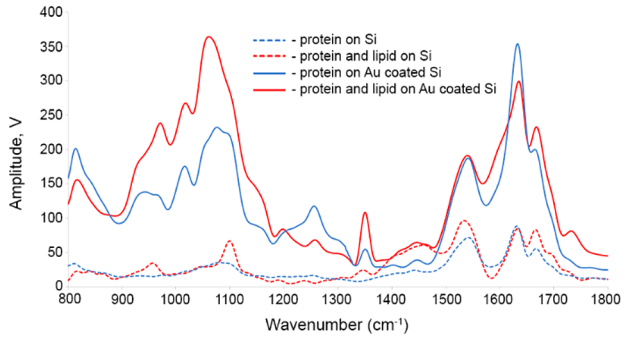

Figure 5. AFM-IR spectra of individual protein aggregates grown in the lipid-free environment (blue) and in the presence of DMPC at 1:1 lipid to protein deposited on Si (dashed lines) and Au-coated Si (solid lines).

Our findings show that amide I region of protein aggregates grown in the lipid-free environment is highly similar in the spectra collected from protein aggregates deposited on bare Si and Au-coated Si substrates. Similar conclusions can be made about amide I region of the protein aggregates grown in the presence of lipids. These aggregates also exhibited vibrational bands that can be assigned to C═C−H (950 cm^{-1}) and PO_2^- (1100 cm^{-1}) vibrations that were not evident in the spectra of the aggregates grown in the lipid-free environment.[42] These two vibrational bands indicate the presence of lipids in the structure of the protein aggregates. At the same time, we have observed drastically different appearance of this region in the spectra collected from the same aggregates deposited on the Au-coated Si substrates. Specifically, we found a set of broad bands around 800, 950, 1050, and 1080 cm^{-1}. We have also found the appearance of new vibrational bands in the 1200−1400 cm^{-1} region that were not observed in the spectra collected from individual protein aggregates deposited on bare Si. These findings show that Au coating can cause significant spectral artifacts in the 800−1400 cm^{-1} region of AFM-IR spectra collected from protein specimens. However, no Au-induced artifacts are observed in the amide I and II regions.

Finally, we measured the total peak area of amide I and II bands (1500−1750 cm^{-1}) in 200 individual AFM-IR spectra of protein aggregates to the surface-enhancement effect, see Figures 6, S1, and S2. Our results show that Au-coating

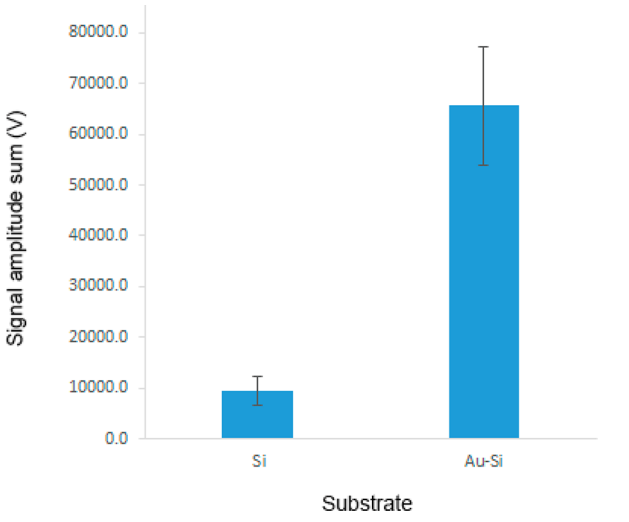

Figure 6. Average intensities of amide I and II bands in AFM-IR spectra collected from protein aggregates deposited on bare Si and a Au-coated Si surface.

provides a factor of 6.83 enhancement to the intensity of this region of IR spectra. Previously, Bibikova and co-workers observed a factor of 10 enhancement of the IR signals of thioglycolic acid (TGA) and up to a factor of 2 enhancement of IR spectra for the bovine serum albumin (BSA) protein induced by anisotropic gold nanostars and spherical gold nanoparticles.[45] Our findings show that Au coating results in a slightly higher enhancement of AFM-IR spectra of protein specimens absorbed onto the metal surface.

CONCLUSIONS

In this study, we examined the surface roughness and IR background of a large number of commercially available substrates to determine their suitability of AFM-IR imaging of small protein aggregates. We found that Si, ZnS, and CaF_2 exhibit the lowest surface roughness simultaneously, providing a very low IR background. This makes them suitable for AFM-IR imaging of aggregates that were grown in the lipid-free environment. We also found that Au-coating of Si, ZnS, and CaF_2 substrates results in the appearance of the strong background in the 950−1250 cm^{-1} spectral region. Thus, Au-coated substrates can most likely not be used for AFM-IR imaging of lipid-containing protein aggregates. At the same time, our results show that Au coating provides a factor of ∼7 enhancement to the IR signal compared to the intensity of the IR spectra collected from amyloid aggregates deposited on bare Si. It should be noted that a rapid development of lithography and soft science results in the appearance of a large number of novel substrates on the market that could not be tested in this work. Nevertheless, we anticipate that these findings will be of a great importance to a large community of IR spectroscopists that work with protein aggregates, as well as researchers who utilize AFM-IR in biology.

ASSOCIATED CONTENT

Supporting Information

The Supporting Information is available free of charge at https://pubs.acs.org/doi/10.1021/acs.jpcc.1c09643.

https://doi.org/10.1021/acs.jpcc.1c09643
J. Phys. Chem. C XXXX, XXX, XXX−XXX

Specification of the analyzed substrates according to the information provided by the vendor and results of the extensive analysis of the substrate surfaces are presented in Tables S1 and S2. Topography, chemical map, and height distribution of amyloid β oligomers are shown in Figures S1 and S2. Standard deviations of the spectra collected on Si and Au-coated Si are shown in Figure S3 (PDF)

AUTHOR INFORMATION

Corresponding Author

Dmitry Kurouski − *Department of Biochemistry and Biophysics, Texas A&M University, College Station, Texas 77843, United States; Department of Biomedical Engineering, Texas A&M University, College Station, Texas 77843, United States;* orcid.org/0000-0002-6040-4213; Phone: 979-458-3778; Email: dkurouski@tamu.edu

Authors

Stanislav Rizevsky − *Department of Biochemistry and Biophysics, Texas A&M University, College Station, Texas 77843, United States; Department of Biotechnology, Binh Duong University, Thu Dau Mot 820000, Vietnam*

Kiryl Zhaliazka − *Department of Biochemistry and Biophysics, Texas A&M University, College Station, Texas 77843, United States*

Tianyi Dou − *Department of Biochemistry and Biophysics, Texas A&M University, College Station, Texas 77843, United States*

Mikhail Matveyenka − *Department of Biochemistry and Biophysics, Texas A&M University, College Station, Texas 77843, United States*

Complete contact information is available at: https://pubs.acs.org/10.1021/acs.jpcc.1c09643

Notes

The authors declare no competing financial interest.

ACKNOWLEDGMENTS

We are grateful to the National Institute of Health for the provided financial support (R35GM142869).

REFERENCES

(1) Contreras, F.; Ermolenkov, A.; Kurouski, D. Infrared Analysis of Hair Dyeing and Bleaching History. *Anal. Method.* **2020**, *12*, 3741−3747.

(2) Giuliano, S.; Mistek-Morabito, E.; Lednev, I. K. Forensic Phenotype Profiling Based on the Attenuated Total Reflection Fourier Transform-Infrared Spectroscopy of Blood: Chronological Age of the Donor. *ACS Omega* **2020**, *5*, 27026−27031.

(3) Qu, J.-H.; Liu, D.; Cheng, J.-H.; Sun, D.-W.; Ma, J.; Pu, H.; Zeng, X.-A. Applications of near-Infrared Spectroscopy in Food Safety Evaluation and Control: A Review of Recent Research Advances. *Crit. Rev. Food. Sci. Nutr.* **2015**, *55*, 1939−1954.

(4) Heise, H. M., Medical Applications of Infrared Spectroscopy. Progress in Fourier Transform Spectroscopy. *Mikrochimica Acta Supplement*; Springer: Vienna, 1997; Vol. *14*.

(5) Farber, C.; Li, J.; Hager, E.; Chemelewski, R.; Mullet, J.; Rogachev, A. Y.; Kurouski, D. Complementarity of Raman and Infrared Spectroscopy for Structural Characterization of Plant Epicuticular Waxes. *ACS Omega* **2019**, *4*, 3700−3707.

(6) Sakudo, A. Near-Infrared Spectroscopy for Medical Applications: Current Status and Future Perspectives. *Clin. Chim. Acta* **2016**, *455*, 181−188.

(7) Kurouski, D. Advances of Vibrational Circular Dichroism (Vcd) in Bioanalytical Chemistry. A Review. *Anal. Chim. Acta* **2017**, *990*, 54−66.

(8) Nafie, L. A. *Vibrational Optical Activity: Principles and Applications*; Wiley: Chichester, 2011.

(9) Krimm, S. Infrared Spectra and Chain Conformation of Proteins. *J. Mol. Biol.* **1962**, *4*, 528−40.

(10) Socrates, G. *Infrared and Raman Characteristic Group Frequencies*, 3rd ed.; Wiley: New York, 2001; p 334.

(11) Yan, H.; Xu, Y.-C.; Siesler, H. W.; Han, B.-X.; Zhang, G.-Z. Hand-Held near-Infrared Spectroscopy for Authentication of Fengdous and Quantitative Analysis of Mulberry Fruits. *Front. Plant Sci.* **2019**, *10*, na.

(12) Yan, H.; Han, B.-X.; Siesler, H. W. Handheld near-Infrared Spectrometers: Reality and Empty Promises. *Spectroscopy* **2020**, *35*, 15−18.

(13) Schnell, M.; Mittal, S.; Falahkheirkhah, K.; Mittal, A.; Yeh, K.; Kenkel, S.; Kajdacsy-Balla, A.; Carney, P. S.; Bhargava, R. All-Digital Histopathology by Infrared-Optical Hybrid Microscopy. *Proc. Natl. Acad. Sci. U. S. A.* **2020**, *117*, 3388−3396.

(14) Woess, C.; Unterberger, S. H.; Roider, C.; Ritsch-Marte, M.; Pemberger, N.; Cemper-Kiesslich, J.; Hatzer-Grubwieser, P.; Parson, W.; Pallua, J. D. Assessing Various Infrared (Ir) Microscopic Imaging Techniques for Post-Mortem Interval Evaluation of Human Skeletal Remains. *PLoS One* **2017**, *12*, e0174552.

(15) Dazzi, A.; Prater, C. B. Afm-Ir: Technology and Applications in Nanoscale Infrared Spectroscopy and Chemical Imaging. *Chem. Rev.* **2017**, *117*, 5146−5173.

(16) Dazzi, A.; Glotin, F.; Carminati, R. Theory of Infrared Nanospectroscopy by Photothermal Induced Resonance. *J. Appl. Phys.* **2010**, *107*, 124519.

(17) Dazzi, A.; Prater, C. B.; Hu, Q. C.; Chase, D. B.; Rabolt, J. F.; Marcott, C. Afm-Ir: Combining Atomic Force Microscopy and Infrared Spectroscopy for Nanoscale Chemical Characterization. *Appl. Spectrosc.* **2012**, *66*, 1365−1384.

(18) Centrone, A. Infrared Imaging and Spectroscopy Beyond the Diffraction Limit. *Annu. Rev. Anal. Chem.* **2015**, *8*, 101−126.

(19) Kurouski, D.; Dazzi, A.; Zenobi, R.; Centrone, A. Infrared and Raman Chemical Imaging and Spectroscopy at the Nanoscale. *Chem. Soc. Rev.* **2020**, *49*, 3315−3347.

(20) Chae, J.; An, S.; Ramer, G.; Stavila, V.; Holland, G.; Yoon, Y.; Talin, A. A.; Allendorf, M.; Aksyuk, V. A.; Centrone, A. Nanophotonic Atomic Force Microscope Transducers Enable Chemical Composition and Thermal Conductivity Measurements at the Nanoscale. *Nano Lett.* **2017**, *17*, 5587−5594.

(21) Chae, J.; Lahiri, B.; Centrone, A. Engineering near-Field Seira Enhancements in Plasmonic Resonators. *ACS Photonics* **2016**, *3*, 87−95.

(22) Katzenmeyer, A. M.; Aksyuk, V.; Centrone, A. Nanoscale Infrared Spectroscopy: Improving the Spectral Range of the Photothermal Induced Resonance Technique. *Anal. Chem.* **2013**, *85*, 1972−1979.

(23) Ramer, G.; Aksyuk, V. A.; Centrone, A. Quantitative Chemical Analysis at the Nanoscale Using the Photothermal Induced Resonance Technique. *Anal. Chem.* **2017**, *89*, 13524−13531.

(24) Ramer, G.; Ruggeri, F. S.; Levin, A.; Knowles, T. P. J.; Centrone, A. Determination of Polypeptide Conformation with Nanoscale Resolution in Water. *ACS Nano* **2018**, *12*, 6612−6619.

(25) Kochan, K.; Perez-Guaita, D.; Pissang, J.; Jiang, J. H.; Peleg, A. Y.; McNaughton, D.; Heraud, P.; Wood, B. R. In Vivo Atomic Force Microscopy-Infrared Spectroscopy of Bacteria. *J. Royal Soc. Interface* **2018**, *15*, 20180115.

(26) Ruggeri, F. S.; Mannini, B.; Schmid, R.; Vendruscolo, M.; Knowles, T. P. J. Single Molecule Secondary Structure Determination of Proteins through Infrared Absorption Nanospectroscopy. *Nat. Commun.* **2020**, *11*, 2945.

(27) Pancani, E.; Mathurin, J.; Bilent, S.; Bernet-Camard, M. F.; Dazzi, A.; Deniset-Besseau, A.; Gref, R. High-Resolution Label-Free

Detection of Biocompatible Polymeric Nanoparticles in Cells. *Part. Part. Syst. Char.* **2018**, *35*, 1700457.
(28) Mathurin, J.; Pancani, E.; Deniset-Besseau, A.; Kjoller, K.; Prater, C. B.; Gref, R.; Dazzi, A. How to Unravel the Chemical Structure and Component Localization of Individual Drug-Loaded Polymeric Nanoparticles by Using Tapping Afm-Ir. *Analyst* **2018**, *143*, 5940−5949.
(29) Chae, J.; Dong, Q.; Huang, J.; Centrone, A. Chloride Incorporation Process in Ch(3)Nh(3)Pbi(3-X)Cl(X) Perovskites Via Nanoscale Bandgap Maps. *Nano Lett.* **2015**, *15*, 8114−21.
(30) Yoon, Y.; Chae, J.; Katzenmeyer, A. M.; Yoon, H. P.; Schumacher, J.; An, S.; Centrone, A.; Zhitenev, N. Nanoscale Imaging and Spectroscopy of Band Gap and Defects in Polycrystalline Photovoltaic Devices. *Nanoscale* **2017**, *9*, 7771−7780.
(31) Perez-Guaita, D.; Kochan, K.; Batty, M.; Doerig, C.; Garcia-Bustos, J.; Espinoza, S.; McNaughton, D.; Heraud, P.; Wood, B. R. Multispectral Atomic Force Microscopy-Infrared Nano-Imaging of Malaria Infected Red Blood Cells. *Anal. Chem.* **2018**, *90*, 3140−3148.
(32) Ruggeri, F. S.; Longo, G.; Faggiano, S.; Lipiec, E.; Pastore, A.; Dietler, G. Infrared Nanospectroscopy Characterization of Oligomeric and Fibrillar Aggregates During Amyloid Formation. *Nat. Commun.* **2015**, *6*, 7831.
(33) Ruggeri, F. S.; Vieweg, S.; Cendrowska, U.; Longo, G.; Chiki, A.; Lashuel, H. A.; Dietler, G. Nanoscale Studies Link Amyloid Maturity with Polyglutamine Diseases Onset. *Sci. Rep.* **2016**, *6*, 31155.
(34) Ruggeri, F. S.; Benedetti, F.; Knowles, T. P. J.; Lashuel, H. A.; Sekatskii, S.; Dietler, G. Identification and Nanomechanical Characterization of the Fundamental Single-Strand Protofilaments of Amyloid Alpha-Synuclein Fibrils. *Proc. Natl. Acad. Sci. U. S. A.* **2018**, *115*, 7230−7235.
(35) Rizevsky, S.; Kurouski, D. Nanoscale Structural Organization of Insulin Fibril Polymorphs Revealed by Atomic Force Microscopy-Infrared Spectroscopy (Afm-Ir). *Chembiochem* **2020**, *21*, 481−485.
(36) Dou, T.; Li, Z.; Zhang, J.; Evilevitch, A.; Kurouski, D. Nanoscale Structural Characterization of Individual Viral Particles Using Atomic Force Microscopy Infrared Spectroscopy (Afm-Ir) and Tip-Enhanced Raman Spectroscopy (Ters). *Anal. Chem.* **2020**, *92*, 11297−11304.
(37) Chen, S. W.; et al. Structural Characterization of Toxic Oligomers That Are Kinetically Trapped During Alpha-Synuclein Fibril Formation. *Proc. Natl. Acad. Sci. U. S. A.* **2015**, *112*, E1994−2003.
(38) Cremades, N.; et al. Direct Observation of the Interconversion of Normal and Toxic Forms of Alpha-Synuclein. *Cell* **2012**, *149*, 1048−59.
(39) Ruggeri, F. S.; Charmet, J.; Kartanas, T.; Peter, Q.; Chia, S.; Habchi, J.; Dobson, C. M.; Vendruscolo, M.; Knowles, T. P. J. Microfluidic Deposition for Resolving Single-Molecule Protein Architecture and Heterogeneity. *Nat. Commun.* **2018**, *9*, 3890.
(40) Ruggeri, F. S.; Flagmeier, P.; Kumita, J. R.; Meisl, G.; Chirgadze, D. Y.; Bongiovanni, M. N.; Knowles, T. P. J.; Dobson, C. M. The Influence of Pathogenic Mutations in Alpha-Synuclein on Biophysical and Structural Characteristics of Amyloid Fibrils. *ACS Nano* **2020**, *14*, 5213−5222.
(41) Zhou, L.; Kurouski, D. Structural Characterization of Individual Alpha-Synuclein Oligomers Formed at Different Stages of Protein Aggregation by Atomic Force Microscopy-Infrared Spectroscopy. *Anal. Chem.* **2020**, *92*, 6806−6810.
(42) Dou, T.; Zhou, L.; Kurouski, D. Unravelling the Structural Organization of Individual Alpha-Synuclein Oligomers Grown in the Presence of Phospholipids. *J. Phys. Chem. Lett.* **2021**, *12*, 4407−4414.
(43) Galvagnion, C.; Buell, A. K.; Meisl, G.; Michaels, T. C.; Vendruscolo, M.; Knowles, T. P.; Dobson, C. M. Lipid Vesicles Trigger Alpha-Synuclein Aggregation by Stimulating Primary Nucleation. *Nat. Chem. Biol.* **2015**, *11*, 229−34.
(44) Wang, R.; Kurouski, D. Thermal Reshaping of Gold Microplates: Three Possible Routes and Their Transformation Mechanisms. *ACS Appl. Mater. Interfaces* **2019**, *11*, 41813−41820.
(45) Bibikova, O.; Haas, J.; Lopez-Lorente, A. I.; Popov, A.; Kinnunen, M.; Ryabchikov, Y.; Kabashin, A.; Meglinski, I.; Mizaikoff, B. Surface Enhanced Infrared Absorption Spectroscopy Based on Gold Nanostars and Spherical Nanoparticles. *Anal. Chim. Acta* **2017**, *990*, 141−149.

https://doi.org/10.1021/acs.jpcc.1c09643
J. Phys. Chem. C XXXX, XXX, XXX−XXX